Non-Hermitian delocalization and eigenfunctions

Naomichi Hatano

Theoretical Division, MS-B262, Los Alamos National Laboratory, Los Alamos, New Mexico 87545

David R. Nelson

Lyman Laboratory of Physics, Harvard University, Cambridge, Massachusetts 02138

(Received 15 May 1998)

Recent literature on delocalization in non-Hermitian systems has stressed criteria based on sensitivity of eigenvalues to boundary conditions and the existence of a nonzero current. We emphasize here that delocalization *also* shows up clearly in eigenfunctions, provided one studies the product of left and right eigenfunctions, as required on physical grounds, and *not* simply the squared modulii of the eigenfunctions themselves. We also discuss the right and left eigenfunctions of the ground state in the delocalized regime and suggest that the behavior of these functions, when considered separately, may be viewed as ''intermediate'' between localized and delocalized. [S0163-1829(98)03937-X]

I. INTRODUCTION

A delocalization phenomenon in a particularly simple class of non-Hermitian random system has attracted considerable attention recently.[1–19] Among the more recent work is a report by Silvestrov, based on an analysis of eigenfunctions, which claims that the phenomenon studied was not actually delocalization, but ''localization of a very unusual kind.'' Although Silvestrov subsequently revised his views, he still maintains that ''the transition from real to complex spectra in one-dimensional (1D) disordered systems with (an) imaginary vector potential is not a delocalization transition.''[20] In this paper, we review some basic facts of the non-Hermitian delocalization (Sec. II) and then take issue with Silvestrov's interpretation. We stress in Sec. III that the criteria for delocalization used in Refs. 1 and 2 are entirely consistent with a conventional one based on eigenfunctions, provided one studies the correct physical quantity, namely the product of the left and right eigenfunctions associated with a given state. In Sec. IV, we comment on the interesting results of Silvestrov for left and right eigenfunctions considered separately for large asymmetry parameter. We show for the ground state that the results are related to earlier results obtained for charge-density waves[3] and population biology.[12] From this viewpoint, we argue that the behavior of the left and the right eigenfunctions is ''intermediate'' between localized and delocalized behavior.

II. NON-HERMITIAN DELOCALIZATION: EIGENVALUES AND CURRENT

Let us first review some basic facts about non-Hermitian delocalization. A typical example of the systems in question is the one-particle Hamiltonian

$$\mathcal{H} = \frac{(p+ig)^2}{2m} + V(x), \qquad (1)$$

where p is the momentum operator $-i\hbar d/dx$, g is a non-Hermitian field constant in time and space, and $V(x)$ is a random potential. Its lattice version is given by the matrix

$$\mathcal{H}_{xx'} = -\frac{t}{2}(e^{\bar{g}}\delta_{x,x'+1} + e^{-\bar{g}}\delta_{x,x'-1}) + V_x\delta_{x,x'}, \qquad (2)$$

where x and x' here are site indices, V_x is a random potential, and $\bar{g} = ga/\hbar$ with a denoting the lattice spacing. For simplicity, we focus on the one-dimensional case throughout this paper. Periodic boundary conditions are imposed except where stated otherwise. The above Hamiltonian reduces to the Anderson localization problem for $g=0$; in this case, it is widely believed that all eigenfunctions are localized in one and two dimensions.

We showed[1,2] that eigenvalues become complex pair by pair once g is increased beyond a threshold value $g = g_{c1}$ and that the states with complex eigenvalues are delocalized. To show the delocalization, we presented two pieces of evidence. First, we numerically demonstrated that the states with complex eigenvalues carry a current. The current carried by the nth eigenstate is defined by $j_n = \partial\varepsilon_n(g)/\partial(ig)$, where ε_n is the eigenvalue. This is the standard definition of the current, because g in Eqs. (1) and (2) plays the role of imaginary vector potential. The current was clearly nonzero for states in the bubble of complex eigenvalues in the band center [see Fig. 13 of Ref. 2 and Fig. 2(b) below], indicating the delocalization of the states.

As a second indication of delocalization, we showed that the delocalized states have complex eigenvalues for systems with periodic boundaries, but that all eigenvalues remain real when the same system has open boundary conditions. This sensitivity to boundary conditions is another indication that the corresponding wave functions are delocalized. We confirmed these two signatures of delocalization in a sufficiently strong imaginary vector potential with numerical work and analytic calculations on localized impurities.

This delocalization phenomenon is equivalent to flux-line depinning in type-II superconductors with extended defects. Suppose that a superconductor has columnar defects randomly located but mutually parallel and that an external magnetic field forces a flux line into the superconductor. The flux line tends to be pinned by a columnar defect (or a collection of them) when the external field is parallel to the
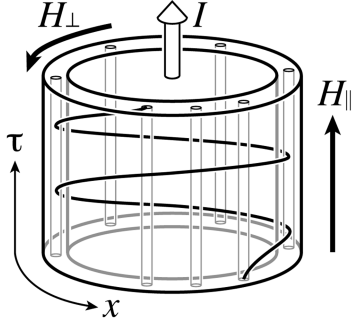
FIG. 1. Vortex-line system characterized by a one-dimensional periodic non-Hermitian transfer matrix. A magnetic field $H_\parallel$ forces a flux line into a cylindrical shell of type-II superconductor with columnar defects. The current threading the cylinder generates the magnetic-field component $H_\perp$, which tries to tilt the flux line. When this flux-line system is mapped onto a ring of the non-Hermitian system, $H_\perp$ becomes proportional to the non-Hermitian field g. Below a certain strength of $H_\perp$ (or g), the flux line is pinned by a columnar defect and forced to run parallel to the defects [the transverse Meissner effect (Ref. 24)], except for its slight deflection from the pinning center near the top and the bottom of the cylinder (Ref. 2). For large enough $H_\perp$, however, the flux line is depinned and wraps around the cylinder as is shown here as a helix. This gives rise to a nonzero current that circulates around the ring of the corresponding non-Hermitian system.

defects. When the field is tilted away from the axis of the defects, we expect flux-line depinning at a certain tilt angle (Fig. 1); see Refs. 21–23 for experiments.

The physics of vortex matter can be mapped onto quantum systems with one less dimension by the inverse of the Feynman path-integral mapping;[24] that is, we regard the Boltzmann weight of the flux line as an exponentiated action of the world line of a quantum particle and make the identification $\hbar \leftrightarrow T$, where T is the temperature of the vortex system. This procedure gives Hamiltonians of the above type. The component of the external magnetic field perpendicular to the columns is proportional to the non-Hermitian field g. Depinning of the flux line by tilting the field beyond a certain strength of g leads to a nonzero current in the corresponding quantum state.[2]

III. NON-HERMITIAN DELOCALIZATION: WAVE FUNCTIONS

Delocalization of the eigenfunctions themselves was not studied directly in Refs. 1 and 2. The main purpose of the present paper is to address this issue.

Silvestrov computed the right eigenfunctions associated with the model (2) for a 300-site lattice in the region of complex eigenvalues and found that their squared moduli have a sparse set of well-separated peaks, quite different from a conventional delocalized state.[20] However, as shown in Ref. 2, and eventually acknowledged by Silvestrov,[20] it is the product of left and right eigenvectors which determines the probability distribution for a tilted vortex line interacting with columnar defects deep within the sample. It is this product which clearly delocalizes in the conventional sense when the eigenvalues become complex. In the hope of avoiding further confusion, we first summarize in this section the ba-

sic relation between left and right eigenvectors. We then illustrate the delocalization of their product with numerical examples from our own extensive 1000-site-lattice computations.

A. Left and right eigenfunctions

We work for concreteness with the continuum Hamiltonian (1), but the results also apply to lattice non-Hermitian models like Eq. (2). Suppose we have computed a set $\{\phi_n^R(x;g)\}$ of right eigenfunctions of $\mathcal{H}(g)$ which satisfy

$$\mathcal{H}(g)|n;g\rangle = \varepsilon_n(g)|n;g\rangle, \tag{3}$$

where we adopt the Dirac bra-ket notation,

$$\phi_n^R(x;g) \rightarrow |n;g\rangle. \tag{4}$$

Although left eigenvectors need not be simply related to right eigenvectors in general, there is a particularly simple relation for the Hamiltonian (1), which arises due to the symmetry[2]

$$\mathcal{H}^\dagger(g) = \mathcal{H}(-g), \tag{5}$$

where $\dagger$ denotes the usual Hermitian conjugate. Indeed, as shown below, left eigenvectors can be obtained from right eigenvectors by complex conjugation and letting $g \rightarrow -g$,

$$\phi_n^L(x;g) = \phi_n^R(x;-g)^*, \tag{6}$$

or in Dirac notation,

$$\phi_n^L(x;g) \rightarrow \langle n;g| \equiv |n;-g\rangle^\dagger, \tag{7}$$

where $\dagger$ again denotes conventional Hermitian conjugation. Our convention that the left eigenvector $\langle n;g|$ is defined to be the Hermitian conjugate of $|n;-g\rangle$, *not* of $|n;g\rangle$, allows manipulations which parallel closely those of conventional quantum mechanics. To see that $\langle n;g|$ is in fact a left eigenfunction, we calculate

$$\langle n;g|\mathcal{H}(g) = (\mathcal{H}(g)^\dagger|n;-g\rangle)^\dagger$$
$$= (\mathcal{H}(-g)|n;-g\rangle)^\dagger$$
$$= \langle n;g|\varepsilon_n(-g)^*. \tag{8}$$

Evidently, $\langle n;g|$ will indeed be a left eigenfunction with the *same* eigenvalue as $|n;g\rangle$, provided

$$\varepsilon_n(-g)^* = \varepsilon_n(g). \tag{9}$$

To prove Eq. (9), we let $\mathcal{H}(g)$ act to the right and the left in the matrix element

$$\langle m;g| \mathcal{H}(g) |n;g\rangle \tag{10}$$

and obtain

$$[\varepsilon_m(-g)^* - \varepsilon_n(g)]\langle m;g|n;g\rangle = 0. \tag{11}$$

Equation (9) follows by setting $m=n$, provided $\langle n;g \mid n;g\rangle \neq 0$. More generally, Eq. (11) can be used to show that, with proper normalization, the right and left eigenfunctions form a biorthogonal set,

$$\langle m;g|n;g\rangle = \delta_{m,n}. \tag{12}$$

This set has the usual completeness relation

$$\sum_n |n;g\rangle\langle n;g| = 1. \qquad (13)$$

Equation (9) reduces to the usual Hermitian constraint of real eigenvalues when $g=0$.

Once the eigenvectors are properly normalized, the imaginary-time particle propagator is given by

$$G(\tau) = \sum_n |n;g\rangle\langle n;g| e^{-\varepsilon_n(g)\tau/\hbar}, \qquad (14)$$

or, in the coordinate representation,

$$G(x,x';\tau) = \sum_n \phi_n^R(x)\phi_n^L(x') e^{-\varepsilon_n(g)\tau/\hbar}. \qquad (15)$$

The density distribution of a particle in the ground state (which dominates as $\tau \to \infty$) is hence the product of left and right eigenfunctions, $\phi_{gs}^L(x)\phi_{gs}^R(x)$. As was shown in Ref. 2, this product gives the probability distribution of a flux line far from the sample boundaries in the imaginary-time direction (the top and the bottom edges of the cylinder in Fig. 1). The square moduli $|\phi_n^R(x)|^2$ and $|\phi_n^L(x)|^2$ are *irrelevant* for the bulk properties.

B. Delocalization of $\phi^L\phi^R$

We now illustrate the different behaviors of $|\phi_n^R(x)|^2$, $|\phi_n^L(x)|^2$, and $\phi_n^L(x)\phi_n^R(x)$ with numerical results, emphasizing that the product $\phi_n^L\phi_n^R$ is clearly delocalized in the conventional sense when eigenvalues become complex. We consider a particular realization of the random Hamiltonian (2) on a 1000-site lattice. The parameters are set to $t=2$ and $\bar{g}=0.4$ with the value of V_x at each site chosen randomly from the range $[-1.5,1.5]$. These values are the same as used in Ref. 20 except that the system size is greater in our calculation. (Note that the definition of t differs by a factor of 2.) The energy spectrum is shown in Fig. 2(a). The states between the two mobility edges $\varepsilon_c \simeq \pm 2.34$ have complex eigenvalues (and hence we would argue are delocalized) while the other states are localized. Every delocalized states carries a complex current as is shown in Fig. 2(b). The imaginary part of the current determines the tilt angle of a flux line.[1,2]

Figure 3(a) shows the functions $\phi_n^L(x)\phi_n^R(x)$, $|\phi_n^R(x)|^2$, and $|\phi_n^L(x)|^2$ for the (localized) ground state. All quantities are normalized so that the summation over x yields unity. We stress, however, that the normalization only makes physical sense for $\phi_n^L(x)\phi_n^R(x)$. Everywhere in the regime of localized states,

$$\phi_n^R(x;g) \propto e^{gx/\hbar}\phi_n(x;0)$$

and

$$\phi_n^L(x;g) \propto e^{-gx/\hbar}(\phi_n(x;0))^* \qquad (16)$$

for large enough systems, where $\phi_n(x;0)$ is the wave function of the Hamiltonian with $g=0$. Note that Eq. (6) is obeyed. [The specific g dependence in Eq. (16) *only* holds for localized states, for which we can always choose
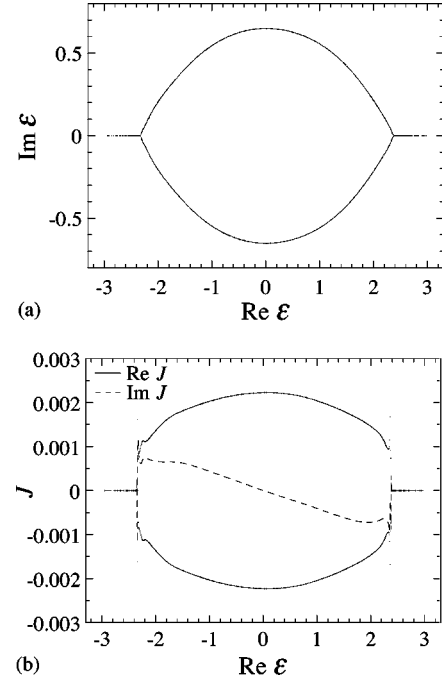

FIG. 2. The complex energy spectrum and the current distribution of the Hamiltonian (2) on a 1000-site lattice. Each eigenvalue is marked by a tiny cross in (a). Each pair of complex conjugate eigenvalues in (a) has the current shown in (b), with the reals part of the opposite sign (tiny crosses) and the identical imaginary parts (the dashed line). The parameters in Eq. (2) are set to $t=2$ and $\bar{g}=0.4$ with each V_x chosen randomly from the range $[-1.5,1.5]$.

$\phi_n(x;0)$ to be real.] Hence, the product $\phi_n^L(x;g)\phi_n^R(x;g) = |\phi_n(x;0)|^2$ does not depend on g until the state is delocalized for large enough g. This is a mathematical expression of the transverse Meissner effect, or the rigidity of the pinned flux line against the tilt of the applied magnetic field; see Refs. 2 and 24 for details.

Figure 3(b) shows the functions $|\phi_n^L(x)\phi_n^R(x)|$, $|\phi_n^R(x)|^2$, and $|\phi_n^L(x)|^2$ for a state slightly below the lower mobility edge, while Fig. 3(c) shows those for a state slightly above the edge. [We only plot the amplitude of the function $\phi_n^L(x)\phi_n^R(x)$; the phase oscillates rapidly for delocalized states away from the band edges.] The function $|\phi_n^L(x)\phi_n^R(x)|$ changes dramatically across the mobility edge, while the changes in $|\phi_n^R(x)|^2$ and $|\phi_n^L(x)|^2$ are less noticeable.

The delocalized nature of $\phi_n^L(x)\phi_n^R(x)$ appears even more dramatically deep inside the bubble of complex eigenvalues. Figure 4(a) shows the same functions for an eigenstate with the eigenvalue $\varepsilon_n = -2.012\,39 + i\,0.200\,376$. This is the 166th state, which roughly corresponds to the 50th state of the 300-site system studied by Silvestrov.[20] In Fig. 4(a), the function $|\phi_n^L(x)\phi_n^R(x)|$ is extended and approximately constant, while $|\phi_n^R(x)|^2$ and $|\phi_n^L(x)|^2$ exhibit a sparse set of well-separated maxima. Following Silvestrov, we plot the logarithm of these functions in Fig. 4(b). The *product* of $\phi^R(x)$ and $\phi^L(x)$ is remarkably constant and is extended in conventional sense. On the other hand, the ragged wandering nature of $\ln|\phi_n^R(x)|$ and $\ln|\phi_n^L(x)|$ is consistent with the conjecture[20] that these functions behave like random walks as a function of x; this is the subject of the next section.
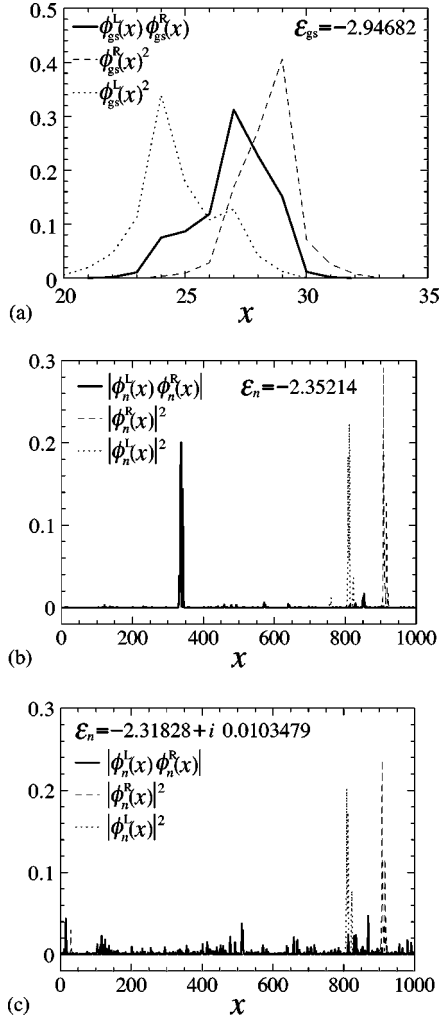
FIG. 3. The functions $|\phi^L(x)\phi^R(x)|$ (thick solid lines), $|\phi^R(x)|^2$ (dashed lines), and $|\phi^L(x)|^2$ (dotted lines) for the following cases: (a) the ground state ($\varepsilon = -2.946\,82$); (b) an eigenstate just below the lower mobility edge (the 72nd state with $\varepsilon = -2.352\,14$); (c) an eigenstate just above the lower mobility edge (the 80th state with $\varepsilon = -2.318\,28 + i\,0.010\,347\,9$). The system is the same as the one used in Fig. 2. The serial number of each state represents the ascending order of the real part of the eigenvalue.
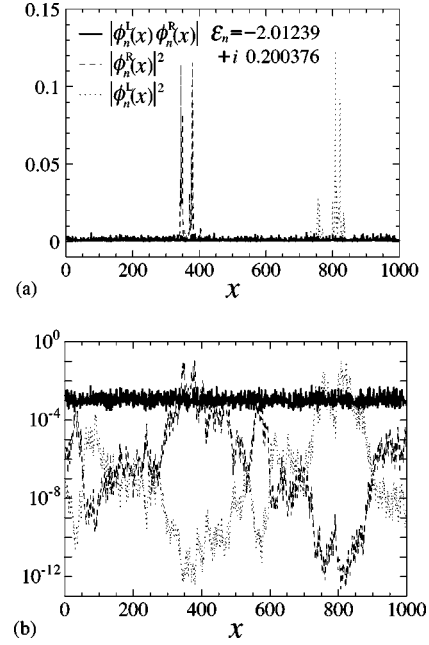

FIG. 4. The functions $|\phi^L(x)\phi^R(x)|$ (thick solid lines), $|\phi^R(x)|^2$ (dashed lines), and $|\phi^L(x)|^2$ (dotted lines) for the eigenstate in the delocalized regime (the 166th state with $\varepsilon = -2.012\,39 + i\,0.200\,376$); (a) a linear plot and (b) a semilogarithmic plot. The system is the same as the one used in Fig. 2.

IV. RANDOM-WALK BEHAVIOR OF EIGENFUNCTIONS

In this section, we turn our attention to the left and right eigenfunctions considered separately for large g. One of the interesting results of Silvestrov[20] is a random-walk-like behavior hidden in the logarithms of the modulii of these eigenfunctions. We first illustrate the random-walk behavior with our more extensive numerical results and then show that, at least for the ground state, Silvestrov's observation is related to earlier results obtained for charge-density waves[3] and population biology.[12] As a concluding remark, we argue that the behavior of sample-to-sample fluctuations of the left and right ground-state eigenfunctions considered separately for large g is ''intermediate'' between that expected for localized and delocalized states.

A. Vortex-line distribution at boundaries

What information is contained in the functions $\phi^R_n(x)$ and $\phi^L_n(x)$ (considered separately) for flux-line systems? For a single vortex line, only the *ground state* contributes in the limit of a very long cylinder. As discussed in Ref. 2 and exploited in a very recent paper by Silvestrov,[25] the (nodeless) ground-state wave functions $\phi^R_{gs}(x)$ and $\phi^L_{gs}(x)$ (*not* their moduli squared) are proportional to the vortex-line probability distribution at the boundaries where it enters and leaves the cylinder (see Fig. 1).

There are then two cases to consider. For small and intermediate values of g, the spectrum is either completely localized or only partially delocalized as in Fig. 2(a). In this case the ground state is localized as in Fig. 3(a), and hence a single vortex line is pinned close to a preferred columnar defect in the bulk of the superconductor cylinder. The right and left eigenfunctions are shifted relative to their product. This reflects the tendency of the localized vortex line to tear away from the pinning center at the top and bottom of the sample when g is nonzero; see Fig. 15(a) of Ref. 2 for a demonstration.

The second more interesting case is for large $g > g_{c2}$, such that *all* states, including the ground state, are delocalized. Using the WKB approximation, Silvestrov[20] argued for random-walk behavior of the logarithm of the wave functions in this case. For concreteness, we show some of our numerical results for the ground state of a 2000-site lattice. (Silvestrov[20] did not show numerical results for the ground state in this regime.) Figure 5(a) shows the ground-state quantities $\phi^L_{gs}(x)$, $\phi^R_{gs}(x)$, and $\phi^L_{gs}(x)\phi^R_{gs}(x)$ for $g = 1.5\hbar/a > g_{c2}$; the values of the other parameters are the same as in the earlier figures. The product $\phi^L_{gs}(x)\phi^R_{gs}(x)$ is approximately constant, while the (nodeless) eigenfunctions $\phi^L_{gs}(x)$ and $\phi^R_{gs}(x)$ are quite different than in Fig. 3(a): They exhibit *multiple* sharp maxima which are rather well separated. In view of these multiple maxima, one might question whether
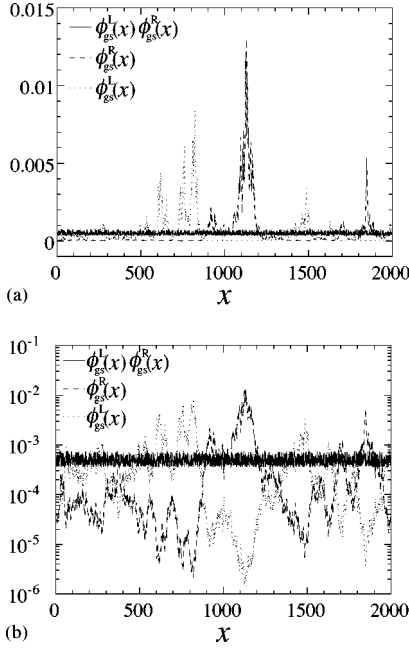
FIG. 5. The functions $\phi^L(x)\phi^R(x)$ (think solid lines), $\phi^R(x)$ (dashed lines), and $\phi^L(x)$ (dotted lines) for the delocalized ground state of a 2000-site lattice; (a) a linear plot and (b) a semilogarithmic plot. All these functions are positive definite in this case. The normalization of $\phi^R(x)$ and $\phi^L(x)$ is different from the one in earlier figures; each is normalized so that its sum over x (not the sum of the squared modulus) becomes unity. The parameter values are the same as the ones used in Fig. 2 except that $\bar{g} = 1.5$.

it is appropriate to call such eigenfunctions "localized."[20] Figure 5(b) shows the same ground-state quantities in a semilogarithmic plot. The wandering, ragged shape of $\ln\phi_{gs}^R(x)$ and $\ln\phi_{gs}^L(x)$ again indicates the random-walk behavior.

The different shapes of $\phi_{gs}^L(x)\phi_{gs}^R(x)$, $\phi_{gs}^R(x)$, and $\phi_{gs}^L(x)$ reflect the different optimization problems of the vortex-line configuration in the bulk, at the top and at the bottom of the superconductor cylinder (see Fig. 1). Since the string tension of the vortex line (the "mass" of the corresponding quantum particle) is missing outside the superconductor, the vortex line can take better advantage of the potential energy at the top and bottom of the sample than in the bulk; hence the sharp maxima in $\phi_{gs}^L(x)$ and $\phi_{gs}^R(x)$. The multiple maxima indicate that the depinned vortex line can enter and exit the superconductor at a variety of preferred locations.

The optimization problems are also different at the top versus the bottom of the cylinder in Fig. 1. When the vortex line enters the sample from below, it is the succession of defects *counterclockwise* to the entry point which are most important. When exiting the sample, it is the defects *clockwise* to the exit point that matter most. Hence the peaks in $\phi_{gs}^L(x)$ and in $\phi_{gs}^R(x)$ appear at very different locations. Nevertheless, the entry and exit probability distributions are strongly correlated with each other, since their product is approximately constant.

B. Renormalization group for the ground state

In the following, let us reproduce Silvestrov's WKB result for delocalized states in a more controlled approxima-

tion. For the ground state, his result is in fact a special case of numerical, scaling, and renormalization-group calculations applied previously to related problems in one-dimensional charge-density waves[3] and population biology in d dimensions.[12]

We start with the time-dependent Schrödinger equation for the continuum Hamiltonian (1),

$$\hbar \frac{\partial}{\partial \tau} \psi^R(x,\tau) = -\mathcal{H}\psi^R(x,\tau)$$

$$= \frac{1}{2m}\left(\hbar \frac{\partial}{\partial x} - g\right)^2 \psi^R(x,\tau) - V(x)\psi^R(x,\tau). \tag{17}$$

We assume uncorrelated finite-width randomness of the potential,

$$\overline{V(x)V(x')} = \Delta^2 \delta(x-x'), \tag{18}$$

where the overbar denotes the random average and Δ is the width of the random distribution.

The d-dimensional generalization of Eq. (17) was studied in Refs. 3 and 12 via the "Cole-Hopf transformation,"

$$\psi^R(x,\tau) = \exp\left[-\frac{\Phi(x,\tau)}{\hbar} + \frac{g^2}{2m\hbar}\tau\right]. \tag{19}$$

The Cole-Hopf transformation is just another name for the WKB method. The second term in the exponent of Eq. (19) is added in order to offset the ground-state energy (which has no effect in the physics of flux line). The equation for Φ is

$$\frac{\partial \Phi}{\partial \tau} = -\frac{g}{m}\frac{\partial \Phi}{\partial x} + V(x) + \frac{\hbar}{2m}\frac{\partial^2 \Phi}{\partial x^2} - \frac{1}{2m}\left(\frac{\partial \Phi}{\partial x}\right)^2. \tag{20}$$

To see the relevance of each term in the long-distance limit, we change the scale as part of a renormalization-group calculation, according to

$$x = s\tilde{x}, \tag{21}$$

$$\tau = s^z \tilde{\tau}, \tag{22}$$

$$\Phi = s^\alpha \tilde{\Phi}, \tag{23}$$

where the exponents z and α are determined below. Thus we have

$$\frac{\partial \tilde{\Phi}}{\partial \tilde{\tau}} = -s^{z-1}\frac{g}{m}\frac{\partial \tilde{\Phi}}{\partial \tilde{x}} + s^{z-\alpha-1/2}\tilde{V}(\tilde{x})$$

$$+ s^{z-2}\frac{\hbar}{2m}\frac{\partial^2 \tilde{\Phi}}{\partial \tilde{x}^2} - s^{z+\alpha-2}\frac{1}{2m}\left(\frac{\partial \tilde{\Phi}}{\partial \tilde{x}}\right)^2. \tag{24}$$

The rescaled random potential is defined by $\tilde{V}(\tilde{x}) \equiv s^{1/2}V(s\tilde{x})$ so that it satisfies $\overline{\tilde{V}(\tilde{x})\tilde{V}(\tilde{x}')} = \Delta^2 \delta(\tilde{x}-\tilde{x}')$.

The first term of the right-hand side of Eq. (24) is a drift term and the second term is the random potential term. To keep these two terms fixed in the long-distance limit $s \to \infty$, we set $z = 1$ and $\alpha = 1/2$. The third and the fourth terms are then irrelevant variables in a perturbative renormalization

group like that constructed in Ref. 12. Thus a Gaussian fixed point controls the physics of what turns out to be the regime $g > g_{c2}$.

Upon defining renormalized parameters by

$$\tilde{m} = s^{-z-\alpha+2}m, \qquad (25)$$

$$\tilde{\hbar} = s^{-\alpha}\hbar, \qquad (26)$$

$$\tilde{g} = s^{1-\alpha}g, \qquad (27)$$

and

$$\tilde{\Delta} = s^{z-\alpha-1/2}\Delta, \qquad (28)$$

we arrive at a Langevin-type equation in the long-distance limit,

$$\left(\frac{\partial}{\partial\tau} + \frac{g}{m}\frac{\partial}{\partial x}\right)\Phi(x,\tau) = V(x), \qquad (29)$$

where we have dropped the "tilde" symbol from all quantities. Since the ground-state energy was already offset in Eq. (19), we can eliminate the time derivative by moving onto a new set of coordinates as $(x,\tau)\rightarrow[x,\tau-(m/g)x]$. We thus see that the solution is a random walk evolving into the x direction:

$$\Phi(x,\tau) \equiv \Phi(x) = \frac{m}{g}\int^{x} V(x')dx'. \qquad (30)$$

The stationary right eigenfunction in the long-distance limit is hence given by

$$\phi_{gs}^{R}(x) = \exp\left[-\frac{m}{g\hbar}\int^{x} V(x')dx'\right], \qquad (31)$$

except a normalization factor. This is equivalent to the ground-state ($k=0$) solution of Silvestrov's calculations.[20,25] Equations (6) and (31) then give the left eigenfunction as

$$\phi_{gs}^{L}(x) = \exp\left[\frac{m}{g\hbar}\int^{x} V(x')dx'\right]. \qquad (32)$$

Note that the random-walk behavior disappears for the product $\phi_{gs}^{L}\phi_{gs}^{R}$, which is just a constant in this approximation, consistent with the numerical result in Fig. 5 for $g > g_{c2}$.

C. Sample-to-sample fluctuations

Silvestrov[20,25] referred to the above behavior of ϕ_{gs}^{R} and ϕ_{gs}^{L} as "stochastic localization" (or simply as "localization" in some sentences). Although the behavior is quite different than the smooth delocalized behavior of their product, it is not clear to us whether such states should be called "localized" either.

To stress this point further, we follow Refs. 3 and 12 and consider the sample-to-sample fluctuations of the logarithm of the ground-state wave function at a fixed location,

$$W(L_x) \equiv \overline{\ln\phi_{gs}(x)^2} - \overline{\ln\phi_{gs}(x)}^2, \qquad (33)$$
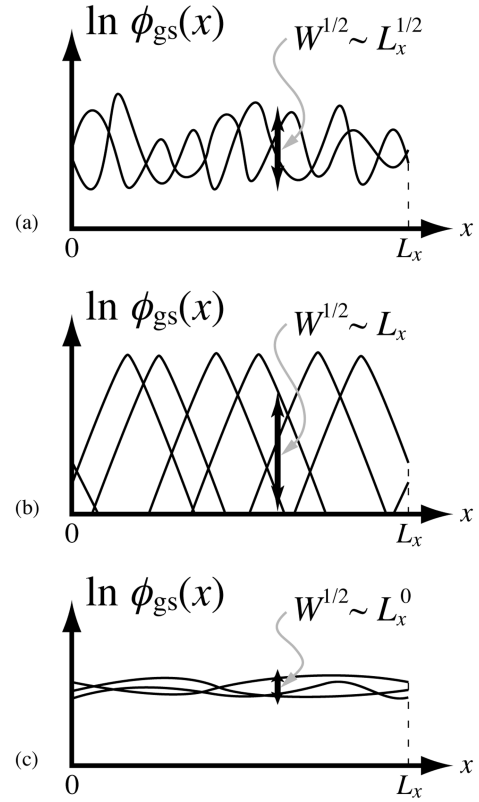

FIG. 6. Schematic views of sample-to-sample fluctuation $W(L_x)$ for various types of ground state: (a) random-walk wave functions of the form (31); (b) a set of wave functions localized in a conventional sense; (c) wave functions which are extended in a conventional sense. Different curves in each graph indicate wave functions of different samples.

where L_x is the system size in the x direction and $\phi_{gs}(x)$ is either the right or the left eigenfunction of the ground state. (We choose a normalization such that $\int\phi_{gs}^{L}\phi_{gs}^{R}dx = 1$.) The x dependence of this quantity should disappear owing to the statistical translational invariance. As is shown below and in Fig. 6, we would have

(i) $W(L_x) \simeq O(L_x)$ for the ground-state wave functions (31) and (32);

(ii) $W(L_x) \simeq O(L_x^2)$ for a conventional (Hermitian) localized ground state;

(iii) $W(L_x) \simeq O(L_x^0)$ for a conventional extended ground state.

From this point of view, the random-walk behavior of ϕ^{R} and ϕ^{L} may be viewed "intermediate" between localized and delocalized.

The first L_x dependence of the quantity $W(L_x)$ is derived either from the wave function (31) or (32) as

$$W(L_x) \propto \iint dx'dx''\overline{V(x')V(x'')} = O(L_x). \qquad (34)$$

Next, to calculate $W(L_x)$ for a conventional localized ground state, we assume its asymptotic form as $\phi(x) \sim \exp(-\kappa|x-x_c|)$ and that the value of κ is approximately equal for all samples but the localization center x_c is different from

sample to sample; see Fig. 6(b). The random average in Eq. (33) then reduces to the average over x_c. Thus we have

$$W(L_x) \sim \frac{\kappa^2}{L_x} \int |x - x_c|^2 dx_c - \left[\frac{\kappa}{L_x} \int |x - x_c| dx_c \right]^2 = O(L_x^2). \tag{35}$$

Finally, the logarithm of a conventional extended ground state should be approximately homogeneous in space for all samples and hence have little sample-to-sample fluctuation as illustrated in Fig. 6(c). This is the behavior of $\phi_{gs}^L \phi_{gs}^R$ when $g > g_{c2}$.

V. SUMMARY

In conclusion, we have argued that, contrary to some recent statements in the literature, delocalization does appear in the eigenfunctions of Hamiltonians such as Eqs. (1) and (2) when the spectrum becomes complex, provided one studies the product of left and right eigenfunctions. Delocalization defined by this criterion is consistent with earlier defi-nitions based on ability of states with complex eigenvalues to carry a nonzero current and the sensitivity to boundary conditions.[1,2]

The left and right eigenfunctions considered separately provide interesting information about the physics of an isolated vortex line at its entry and exit points. Similar conclusions apply to interacting arrays of vortices. See Sec. VIII of Ref. 2 for a discussion of this non-Hermitian many-body problem. An interesting investigation of tilted interacting vortices at the entry and exit boundaries has been initiated by Silvestrov.[25]

[1] N. Hatano and D. R. Nelson, Phys. Rev. Lett. **77**, 570 (1996).

[2] N. Hatano and D. R. Nelson, Phys. Rev. B **56**, 8651 (1997).

[3] L.-W. Chen, L. Balents, M. P. A. Fisher, and M. C. Marchetti, Phys. Rev. B **54**, 12 798 (1996).

[4] N. Shnerb, Phys. Rev. B **55**, R3382 (1997).

[5] K. B. Efetov, Phys. Rev. Lett. **79**, 491 (1997).

[6] J. Feinberg and A. Zee, Nucl. Phys. B **504** [FS], 579 (1997).

[7] R. A. Janik, M. A. Nowak, G. Papp, and I. Zahed, cond-mat/9705098 (unpublished).

[8] P. W. Brouwer, P. G. Silvestrov, and C. W. J. Beenakker, Phys. Rev. B **56**, R4333 (1997).

[9] J. Feinberg and A. Zee, cond-mat/9706218 (unpublished).

[10] I. Ya. Goldsheid and B. A. Khoruzhenko, Phys. Rev. Lett. **80**, 2897 (1998).

[11] E. Brezin and A. Zee, Nucl. Phys. B **509** [FS], 599 (1998).

[12] D. R. Nelson and N. Shnerb, Phys. Rev. E **58**, 1383 (1998).

[13] J. Feinberg and A. Zee, cond-mat/9710040 (unpublished).

[14] R. A. Janik, M. A. Nowak, G. Papp, and I. Zahed, Acta Phys. Pol. B **28**, 2949 (1997).

[15] A. Zee, Physica A **254**, 300 (1998).

[16] N. Hatano, Physica A **254**, 317 (1998).

[17] N. M. Shnerb, Phys. Rev. B **57**, 8571 (1998).

[18] C. Mudry, B. D. Simons, and A. Altland, Phys. Rev. Lett. **80**, 4257 (1998).

[19] N. M. Shnerb and D. R. Nelson, Phys. Rev. Lett. **80**, 5172 (1998).

[20] P. G. Silvestrov, cond-mat/9802219v2, Phys. Rev. B (to be published).

[21] W. Jiang, N.-C. Yeh, D. S. Reed, U. Kriplani, D. A. Beam, M. Konczykowski, T. A. Tombrello, and F. Holtzberg, Phys. Rev. Lett. **72**, 550 (1994).

[22] H. Safar, S. R. Foltyn, Q. X. Jia, and M. P. Maley, Philos. Mag. B **74**, 647 (1996).

[23] I. M. Obaidat, S. J. Park, H. Safar, and J. S. Kouvel, Phys. Rev. B **56**, R5774 (1997).

[24] D. R. Nelson and V. Vinokur, Phys. Rev. B **48**, 13 060 (1993).

[25] P. G. Silvestrov, cond-mat/9804093 (unpublished).